



Control of Robotic Vehicles with Actively Articulated Suspensions in Rough Terrain

KARL IAGNEMMA, ADAM RZEPNIEWSKI AND STEVEN DUBOWSKY

Department of Mechanical Engineering, Massachusetts Institute of Technology, Cambridge, MA 02139, USA

kdi@mit.edu

PAUL SCHENKER

*Science and Technology Development Section, Jet Propulsion Laboratory, California Institute of Technology,
Pasadena, CA 91109, USA*

Abstract. Future robotic vehicles will perform challenging tasks in rough terrain, such as planetary exploration and military missions. Rovers with actively articulated suspensions can improve rough-terrain mobility by repositioning their center of mass. This paper presents a method to control actively articulated suspensions to enhance rover tipover stability. A stability metric is defined using a quasi-static model, and optimized on-line. The method relies on estimation of wheel-terrain contact angles. An algorithm for estimating wheel-terrain contact angles from simple on-board sensors is developed. Simulation and experimental results are presented for the Jet Propulsion Laboratory Sample Return Rover that show the control method yields substantially improved stability in rough-terrain.

Keywords: mobile robots, articulated suspension, robot control, rough terrain, vehicle mobility

1. Introduction

Mobile robotic vehicles are increasingly being proposed for high-risk, rough terrain missions, such as planetary exploration, hazardous site clean-up, and military applications (Golombek, 1998; Shoemaker and Bornstein, 1998). Future planetary exploration missions will require mobile robots to perform difficult mobility tasks in rough terrain (Hayati et al., 1998; Schenker et al., 1997). Such tasks can result in loss of wheel traction, leading to entrapment, loss of stability, and even tipover. Clearly, tipover instability can result in rover damage and total mission failure.

Robots with actively articulated suspensions, sometimes called “reconfigurable robots,” can improve rough-terrain mobility by modifying their suspension configuration and thus repositioning their center of mass. One example of an articulated suspension robot is the Jet Propulsion Laboratory’s Sample Return Rover (SRR), see Fig. 1. The SRR can actively modify its two shoulder joints to change its center of mass loca-

tion and enhance rough terrain mobility (Huntsberger et al., 1999; Iagnemma et al., 2000). For example, when traversing an incline the SRR can adjust angles θ_1 and θ_2 to improve stability, see Fig. 2. It can also reposition its center of mass by moving its manipulator.

Previous researchers have considered the use of articulated suspensions to enhance rough-terrain vehicle mobility (Sreenivasan and Wilcox, 1994; Sreenivasan and Waldron, 1996; Farritor et al., 1998). In Sreenivasan and Wilcox (1994) a control algorithm is developed for the four-wheeled JPL GOFOR and studied in simulation. This algorithm repositions the GOFOR center of mass to improve stability and wheel traction. This work considers only planar vehicle motion. Also, the method is developed for a particular four-wheeled vehicle configuration, and was not demonstrated experimentally. In Sreenivasan and Waldron (1996) articulated suspension control is discussed for the Wheeled Actively Articulated Vehicle (WAAV) to allow difficult mobility maneuvers. Solutions for the WAAV’s specific kinematic structure are presented,

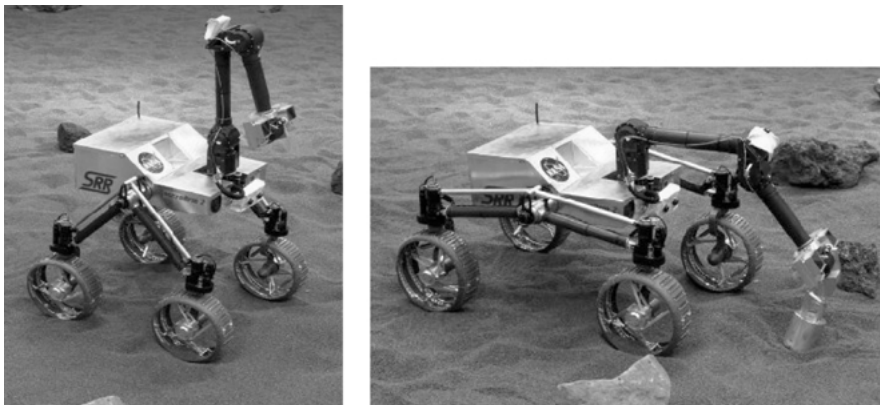


Figure 1. Jet Propulsion Laboratory Sample Return Rover (SRR).

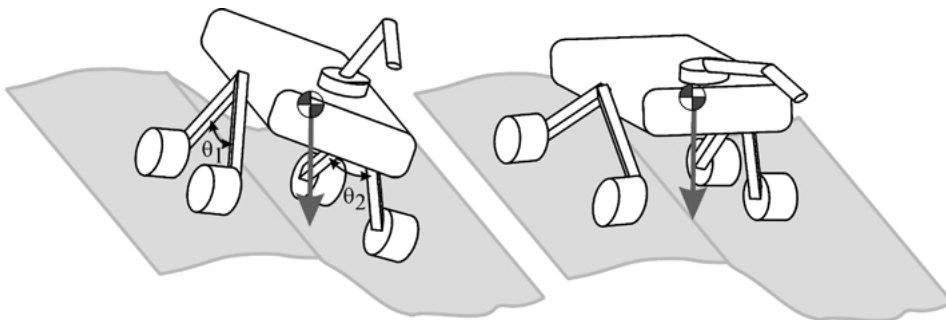


Figure 2. Articulated suspension robot improving stability by adjusting shoulder joints.

and studied in simulation. In Farritor et al. (1998) a genetic algorithm-based method is proposed for repositioning a vehicle's manipulator to modify its center of mass location and aid mobility. This method is computationally intensive and was not validated experimentally.

In this paper a method for stability-based articulated suspension control is presented, and demonstrated experimentally on the JPL SRR. Kinematic equations relating suspension joint variables to a vehicle stability measure are written in closed form. The stability measure considers gravitational forces due to rover weight. It also considers forces due to manipulation, which are potentially large and could have a destabilizing effect on the vehicle. A performance index is defined based on the stability measure and a function that maintains adequate ground clearance, an important consideration in rough terrain. A rapid and computationally practical conjugate-gradient optimization of the performance index is performed subject to vehicle kinematic constraints.

The method does not rely on a detailed terrain map. However, knowledge of the robot's wheel-terrain contact angles is required. In an attempt to measure contact angles, previous researchers have proposed installing multi-axis force sensors at each wheel to measure the contact force direction (Sreenivasan, 1994). The wheel-terrain contact angles could be inferred from the direction of the contact force. However, installing multi-axis force sensors at each wheel is costly and mechanically complex. The complexity reduces reliability and adds weight, two factors that carry severe penalties for space applications. Other researchers have proposed using vehicle models and terrain map data to estimate wheel-terrain contact angles (Balaram, 2000). However, accurate terrain map data is difficult to obtain. Additionally, terrain may deform during robot motion, causing estimation error. In this paper an algorithm is presented that is based on rigid-body kinematic equations, and uses simple on-board sensors such as inclinometers and wheel tachometers to estimate wheel-terrain contact angles (Iagnemma and Dubowsky, 2000). The method

utilizes an extended Kalman filter to fuse noisy sensor signals.

Computational requirements for the wheel-terrain contact angle estimation and suspension control algorithms are light, being compatible with limited on-board computational resources of planetary rovers. Simulation and experimental results for the SRR under field conditions show that articulated suspension control can greatly improve rover stability in rough terrain.

2. The Articulated Suspension Control Problem

Consider a general n -link tree-structured wheeled mobile robot on uneven terrain, see Fig. 3. The n links can form hybrid serial-parallel kinematic chains. It is assumed that the robot's l joints are active revolute or prismatic joints, and their values are denoted θ_i , $i = \{1, \dots, l\}$. It is also assumed that the wheels make point contact with the terrain. This is a reasonable assumption for rigid wheels traveling on firm terrain. The m wheel-terrain contact points are denoted P_j , $j = \{1, \dots, m\}$ with their location defined as a vector \mathbf{p}_j from the vehicle center of mass. The wheel-terrain contact angles at each point P_j are measured with respect to the horizontal axis and are denoted γ_j , $j = \{1, \dots, m\}$.

The goal of articulated suspension control is to improve mobility by modifying the suspension variables θ_i to optimize a user-specified performance index, Φ . This performance index can be selected to assess static stability, wheel traction, vehicle pose for optimal force application, ground clearance, or a combination of metrics, and is generally a function of the suspension and manipulation degrees of freedom. In this paper, static

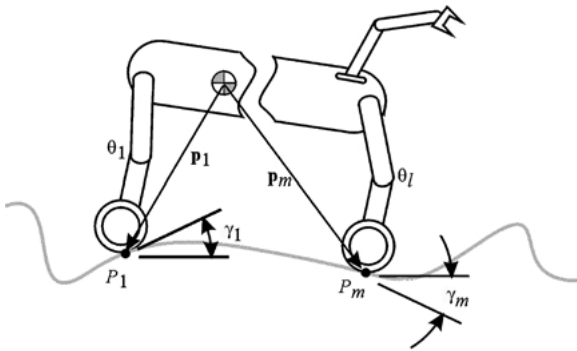


Figure 3. A general tree-structured mobile robot.

stability and ground clearance are optimized in the performance index.

Problem constraints take the form of joint limit and mechanical interference constraints. Constraints also arise from system mobility limitations. These constraints are discussed below.

2.1. Mobility Analysis

The mobility of an articulated suspension robot can be analyzed using the Grubler mobility criterion (Eckhardt, 1989):

$$F = 6(l - j - 1) + \sum_{i=1}^j f_i \quad (1)$$

where j is the number of joints, l is the number of links including the ground, and f_i is the number of constraints for each joint i . Some highly articulated robots may have mobility greater than or equal to one while stationary on the terrain (i.e., the robot has available self-motions). In these situations the terrain profile does not influence the suspension control process. Thus, knowledge of robot kinematics alone is sufficient to pose the optimization problem.

Many articulated suspension robots, however, have a mobility less than or equal to zero. Thus, one or more wheel-terrain contact points P_j must move relative to the terrain during the suspension control process, see Figs. 1 and 2. Note that in such cases, wheel-terrain contacts must be treated as higher-order pairs during mobility analysis (Eckhardt, 1989). In these situations, it is impossible to find a globally optimal solution for the suspension configuration without knowledge of the terrain profile. This is problematic, since the terrain profile is often not well known. However, the local wheel-terrain contact angles can be estimated.

The wheel-terrain contact angle γ_j describes the terrain profile in a local region about the point P_j . An optimization problem can therefore be posed with the constraint that the rover suspension change results in only small displacements of the points P_j relative to the terrain, see Fig. 4. Here we assume that the terrain profile does not change significantly within a small region about the wheel-terrain contact points. Thus, a locally optimal solution for the suspension configuration can be found. Optimization constraints take the form of kinematic joint limit and interference constraints, and joint excursion limits that restrict the displacements of the points P_j .

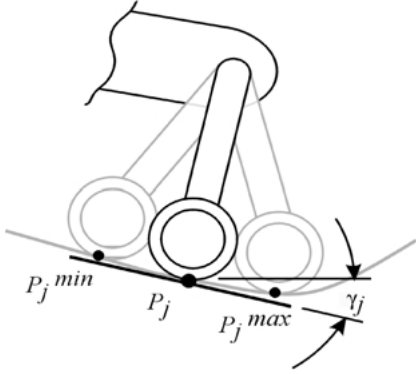


Figure 4. Limited motion of wheel-terrain contact point P_j .

3. Wheel-Terrain Contact Angle Estimation

To perform articulated suspension control, wheel-terrain contact angles are used to approximate the local terrain profile. Here, a method for estimating wheel-terrain contact angles from simple on-board rover sensors is presented.

Consider a planar two-wheeled system on uneven terrain, see Fig. 5. A planar analysis is appropriate since the rover can neither move nor apply forces in the transverse direction. Thus, transverse contact angles are not considered. In this analysis the terrain is assumed to be rigid, and the wheels are assumed to make point contact with the terrain.

For rigid wheels traveling on deformable terrain, the single-point assumption no longer holds. However, an “effective” wheel-terrain contact angle is defined as the angular direction of travel imposed on the wheel by the terrain during motion, see Fig. 6.

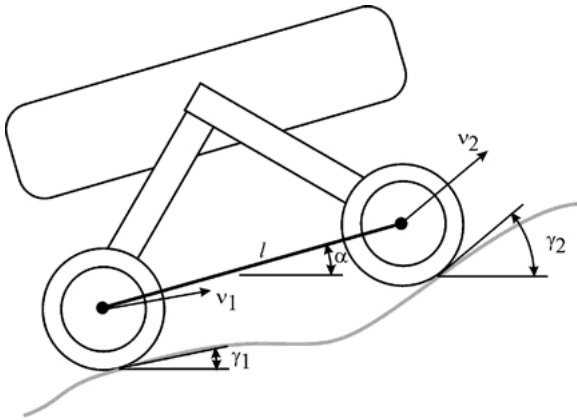


Figure 5. Planar two-wheeled system.

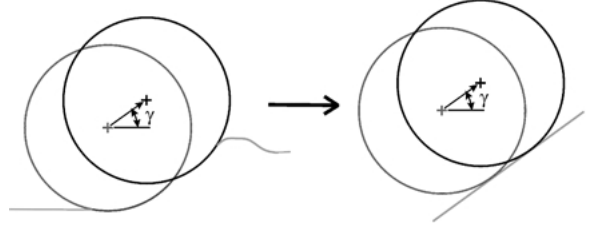


Figure 6. Wheel-terrain contact angle γ for rigid wheel on deformable terrain.

In Fig. 5 the rear and front wheels make contact with the terrain at angles γ_1 and γ_2 from the horizontal, respectively. The vehicle pitch, α , is also defined with respect to the horizontal. The wheel centers have speeds v_1 and v_2 . These speeds are in a direction parallel to the local wheel-terrain tangent due to the rigid terrain assumption. The distance between the wheel centers is defined as l .

For this system, the following kinematic equations can be written:

$$v_1 \cos(\gamma_1 - \alpha) = v_2 \cos(\gamma_2 - \alpha) \quad (2)$$

$$v_2 \sin(\gamma_2 - \alpha) - v_1 \sin(\gamma_1 - \alpha) = l\dot{\alpha} \quad (3)$$

Equation (2) represents the kinematic constraint that the wheel center length l does not change. Note that this constraint remains valid in cases where changes in the vehicle suspension configuration cause changes in l , as long as l varies slowly. Equation (3) is a rigid-body kinematic relation between the velocities of the wheel centers and the vehicle pitch rate $\dot{\alpha}$.

Combining Eqs. (2) and (3) yields:

$$\sin(\gamma_2 - \alpha - (\gamma_1 - \alpha)) = \frac{l\dot{\alpha}}{v_1} \cos(\gamma_2 - \alpha) \quad (4)$$

With the definitions:

$$\theta \equiv \gamma_2 - \alpha, \quad \beta \equiv \alpha - \gamma_1, \quad a \equiv l\dot{\alpha}/v_1, \quad b \equiv v_2/v_1$$

Equations (2) and (4) become:

$$(b \sin \theta + \sin \beta) \cos \theta = a \cos \theta \quad (5)$$

$$\cos \beta = b \cos \theta \quad (6)$$

Solving Eqs. (5) and (6) for the wheel-terrain contact angles γ_1 and γ_2 yields:

$$\gamma_1 = \alpha - \cos^{-1}(h) \quad (7)$$

$$\gamma_2 = \cos^{-1}(h/b) + \alpha \quad (8)$$

where:

$$h \equiv \frac{1}{2a} \sqrt{2a^2 + 2b^2 + 2a^2b^2 - a^4 - b^4 - 1}$$

There are two special cases that must be considered in this analysis. The first special case occurs when the rover is stationary. Equations (5) and (6) do not yield a solution, since if $\dot{\alpha} = v_1 = v_2 = 0$, both a and b are undefined. Physically, the lack of a solution results from the fact that a stationary rover can have an infinite set of possible contact angles at each wheel.

The second special case occurs when $\cos(\theta)$ equals zero. In this case $\gamma_2 = \pm\pi/2 + \alpha$ from the definition of θ , and Eq. (8) yields the solution $\gamma_1 = \pm\pi/2 + \alpha$. Physically this corresponds to two possible cases: the rover undergoing pure translation or pure rotation, see Fig. 7.

While these cases are unlikely to occur in practice, they are easily detectable. For the case of pure rotation, $v_1 = -v_2$. The solutions for γ_1 and γ_2 can be written by inspection as:

$$\gamma_1 = \alpha + \frac{\pi}{2} \text{sgn}(\dot{\alpha}) \quad (9)$$

$$\gamma_2 = \alpha - \frac{\pi}{2} \text{sgn}(\dot{\alpha}) \quad (10)$$

For the case of pure translation, $\dot{\alpha} = 0$, and $v_1 = v_2$. Thus, h is undefined and the system of Eqs. (5) and (6) has no solution. However, for low-speed rovers considered in this work, the terrain profile varies slowly with respect to the data sampling rate. It is reasonable to assume that wheel-terrain contact angles computed at a given timestep will be similar to wheel-terrain contact angles computed at the previous timestep. Thus, previously estimated contact angles can be used when a solution to the estimation equations does not exist.

The pitch and pitch rate can be measured with rate gyroscopes or simple inclinometers. The wheel center speeds can be estimated from the wheel angular rate as measured by a tachometer, provided the wheels do not have substantial slip. Thus, wheel-terrain contact angles can be estimated with common, low-cost on-board sensors. The estimation process is computationally simple, and thus suitable for on-board implementation.

3.1. Extended Kalman Filter Implementation

The above analysis suggests that wheel-terrain contact angles can be computed from simple, measurable quantities. However, sensor noise and wheel slip will degrade these measurements. Here, an extended Kalman filter (EKF) is developed to compensate for these effects. This filter is an effective framework for fusing data from multiple noisy sensor measurements to estimate the state of a nonlinear system (Brown and Hwang, 1997; Welch and Bishop, 1999). In this case the sensor signals are wheel tachometers, gyroscopes, and inclinometers, and are assumed to be corrupted by unbiased Gaussian white noise with known covariance. Again, due to the assumption of quasi-static vehicle motion, inertial effects do not corrupt the sensor measurements. Also, we assume that sensor bandwidth is significantly faster than the vehicle dynamics, and thus sensor dynamics do not corrupt the sensor measurements.

Here we attempt to estimate the state vector \mathbf{x} , composed of the wheel-terrain contact angles, i.e., $\mathbf{x} = [\gamma_1 \ \gamma_2]^T$. The discrete-time equation governing the evolution of \mathbf{x} is:

$$\mathbf{x}_{k+1} = \begin{bmatrix} 1 & 0 \\ 0 & 1 \end{bmatrix} \mathbf{x}_k + \mathbf{w}_k \quad (11)$$

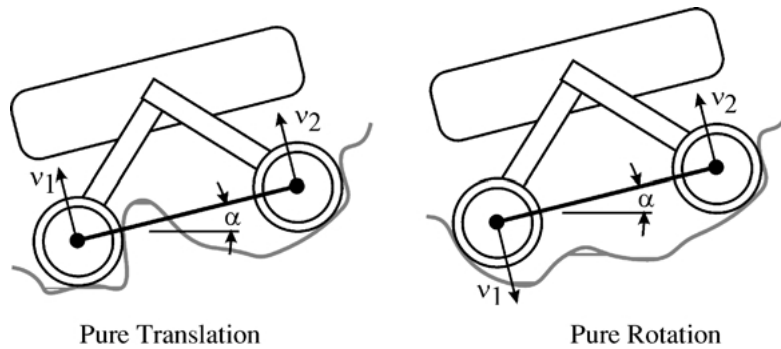


Figure 7. Physical interpretations of $\cos(\theta) = 0$.

where w_k is a 2×1 vector representing the process noise. Equation (11) implies that ground contact angle evolution is a random process. This is physically reasonable, since terrain variation is inherently unpredictable. The elements of w can be assigned as the expected terrain variation:

$$w_k = \mathbb{E}(\mathbf{x}_{k+1} - \mathbf{x}_k) \quad (12)$$

This information could be estimated from knowledge of local terrain roughness, or computed from forward-looking range data.

The EKF measurement equation can be written as:

$$\mathbf{y}_k = \begin{bmatrix} 1 & 0 \\ 0 & 1 \end{bmatrix} \mathbf{x}_k + n_k \quad (13)$$

where \mathbf{y}_k is a synthetic ‘‘measurement’’ of the ground contact angles, computed analytically from Eqs. (7) and (8) and raw sensor data, i.e., $\mathbf{y}_k = f(\mathbf{z}_k)$, where $\mathbf{z} = [\alpha \ \dot{\alpha} \ v_1 \ v_2]^T$. We assume that the vehicle pitch α and pitch rate $\dot{\alpha}$ are directly sensed, and speeds v_1 and v_2 can be approximated from knowledge of the wheel angular velocities and radii. Noise on the sensory inputs is projected onto the ground contact angle measurements through the noise vector n_k , as $n_k \approx \left[\frac{\partial \mathbf{y}_k}{\partial \mathbf{z}} \right]_{\mathbf{z}=\mathbf{z}_k} \cdot [\sigma_\alpha \ \sigma_{\dot{\alpha}} \ \sigma_{v_1} \ \sigma_{v_2}]^T$.

The following is a description of the EKF implementation procedure:

1. Initialization of the state estimate $\hat{\mathbf{x}}_0$ and the estimated error covariance matrix \mathbf{P}_0 . Here, $\hat{\mathbf{x}}_0 = \mathbf{y}_0$, and $\mathbf{P}_0 = \mathbf{R}_x$, where $\mathbf{R}_x = w_0 w_0^T$.
2. Propagation of the current state estimate and covariance matrix. The state estimate is generally computed from a state transition matrix, which here is the identity matrix. Thus:

$$\hat{\mathbf{x}}_k^- = \hat{\mathbf{x}}_{k-1}^- \quad (14)$$

The covariance matrix is computed as:

$$\mathbf{P}_k^- = \mathbf{P}_{k-1}^- + \mathbf{R}_x \quad (15)$$

3. Computation of the Kalman gain, and updating the state estimate and covariance matrix. The Kalman gain matrix \mathbf{K} is given by:

$$\mathbf{K}_k = \mathbf{P}_k^- (\mathbf{P}_k^- + \mathbf{R}_{y_k})^{-1} \quad (16)$$

We can compute the sensor noise matrix \mathbf{R}_{y_k} as:

$$\mathbf{R}_{y_k} = n_k n_k^T = \left(\frac{\partial \mathbf{y}_k}{\partial \mathbf{z}} \right)^T \mathbf{R}_z \left(\frac{\partial \mathbf{y}_k}{\partial \mathbf{z}} \right) \quad (17)$$

where \mathbf{R}_z is a 4×4 diagonal matrix of known noise covariances associated with \mathbf{z} : $\mathbf{R}_z = \text{diag}(\sigma_\alpha^2, \sigma_{\dot{\alpha}}^2, \sigma_{v_1}^2, \sigma_{v_2}^2)$. Note that estimates of \mathbf{R}_{y_k} and \mathbf{y}_k can be formed by computing the Unscented Transform of Eqs. (7) and (8) (Julier and Uhlmann, 1997).

The state estimate is updated as:

$$\hat{\mathbf{x}}_k = \hat{\mathbf{x}}_k^- + \mathbf{K}_k (\mathbf{y}_k - \hat{\mathbf{x}}_k^-) \quad (18)$$

and the covariance matrix is updated as:

$$\mathbf{P}_k = (\mathbf{I} - \mathbf{K}_k) \mathbf{P}_k^- \quad (19)$$

The special cases discussed in Section 3 can lead to a lack of observability in the filter. However, as described above, these situations are easily detectable. Thus, new measurement updates for the filter are not taken when these special cases are detected.

See Fig. 8 for a pictorial diagram of the EKF estimation process (adapted from Welch and Bishop, 1999).

4. Articulated Suspension Control for Enhanced Tipover Stability

Articulated suspension control can be used to improve criteria such as tipover stability or traction. In this section a method for enhancing static stability is described. The static analysis is valid since planetary rovers travel at maximum speeds of only several cm/sec.

In this work, vehicle stability is defined in a manner similar to that proposed in (Papadopoulos and Rey, 1996). For the general mobile robot shown in Fig. 3, m wheel-terrain contact points P_j , $j = \{1, \dots, m\}$ are numbered in ascending order in a clockwise manner when viewed from above, see Fig. 9. The lines joining the wheel-terrain contact points are referred to as tipover axes and denoted \mathbf{a}_i , where the i th tipover axis is given by:

$$\mathbf{a}_i = \mathbf{p}_{i+1} - \mathbf{p}_i, \quad i = \{1, \dots, m-1\} \quad (20)$$

$$\mathbf{a}_m = \mathbf{p}_1 - \mathbf{p}_m \quad (21)$$

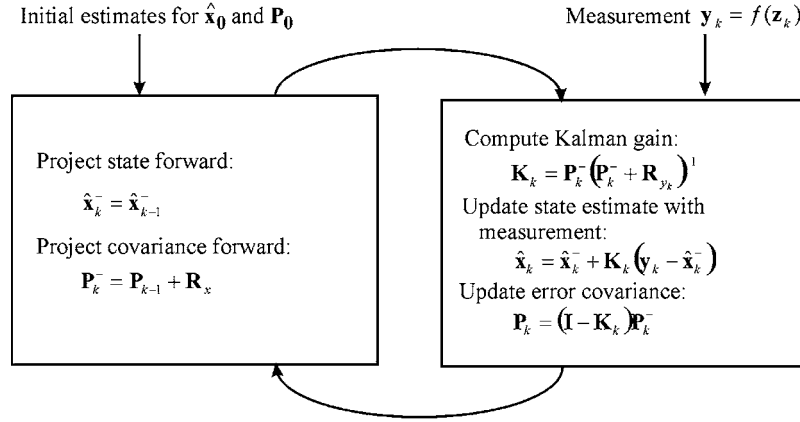


Figure 8. Diagram of EKF estimation process (from Welch and Bishop, 1999).

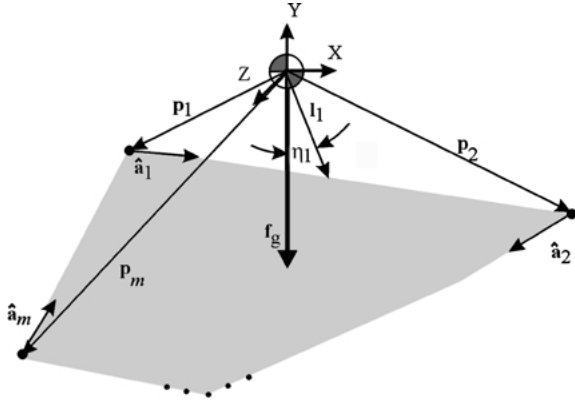


Figure 9. Stability definition diagram.

A vehicle with m wheels or feet in contact with the terrain has in general m tipover axes. Tipover axis normals \mathbf{l}_i that intersect the center of mass can be described as:

$$\mathbf{l}_i = (\mathbf{1} - \hat{\mathbf{a}}_i \hat{\mathbf{a}}_i^T) \mathbf{p}_{i+1} \quad (22)$$

where $\hat{\mathbf{a}} = \mathbf{a}/\|\mathbf{a}\|$. Stability angles can then be computed for each tipover axis as the angle between the gravitational force vector \mathbf{f}_g and the axis normal \mathbf{l}_i :

$$\eta_i = \sigma_i \cos^{-1}(\hat{\mathbf{f}}_g \cdot \hat{\mathbf{l}}_i), \quad i = \{1, \dots, m\} \quad (23)$$

with

$$\sigma_i = \begin{cases} +1 & (\hat{\mathbf{l}}_i \times \hat{\mathbf{f}}_g) \cdot \hat{\mathbf{a}}_i < 0 \\ -1 & \text{otherwise} \end{cases} \quad (24)$$

The overall vehicle stability angle is defined as the minimum of the m stability angles:

$$\beta = \min(\eta_i), \quad i = \{1, \dots, m\} \quad (25)$$

When $\beta < 0$ a tipover instability occurs. Measurements of the wheel contact forces or articulation torques are not required, as this is a kinematics-based stability analysis. Thus, the goal of articulated suspension control is to maintain a large value of β .

In addition to traversing rough terrain, a rover may be required to manipulate its environment. Some manipulation tasks, such as coring, may require the application of large forces, which can destabilize the robot. During these tasks it would be desirable for the rover to optimize its suspension to maximize stability.

To account for manipulation forces in the stability computation, the applied force \mathbf{f}_m is projected along a tipover axis as:

$$\mathbf{f}_i = (\mathbf{1} - \hat{\mathbf{a}}_i \hat{\mathbf{a}}_i^T) (\mathbf{f}_g + \mathbf{f}_m) \quad (26)$$

with \mathbf{f}_m expressed in an inertial frame. If there is a moment \mathbf{n}_m associated with \mathbf{f}_m , the net force about a tipover axis is computed as:

$$\mathbf{f}_i = (\mathbf{1} - \hat{\mathbf{a}}_i \hat{\mathbf{a}}_i^T) (\mathbf{f}_g + \mathbf{f}_m) + \frac{\hat{\mathbf{l}}_i \times (\hat{\mathbf{a}}_i \hat{\mathbf{a}}_i^T) \mathbf{n}_m}{\|\mathbf{l}_i\|} \quad (27)$$

The stability angle β is then computed from Eqs. (23–25) using the net force \mathbf{f}_i in place of \mathbf{f}_g .

To optimize the rover suspension for maximum stability, a performance index Φ is defined based on the

above stability measure. A function of the following form is proposed:

$$\Phi = \sum_{i=1}^n \left(\frac{K_i}{\eta_i} + K_{n+i}(\theta_i - \theta'_i)^2 \right) \quad (28)$$

where η_i are the stability angles defined in Eqs. (23–24), θ'_i are the nominal values of the i th joint variables (i.e., the values of θ_i when the robot is at a user-specified configuration, such as on flat terrain), and K_i are constant weighting factors.

The first term of Φ tends to infinity as the stability at any tipover axis tends to zero. The second term penalizes deviation from a nominal configuration of the suspension. This term is used to maintain adequate ground clearance, an important consideration in rough terrain. Note that an explicit guarantee of ground clearance would require analysis of 3-d terrain range data immediately in front of the vehicle. This method is intended to be reactive in nature, and thus forward-looking range information is not considered. The constants K_i are selected to control the relative importance of vehicle stability and joint excursion.

The goal of the optimization is to minimize the performance index Φ subject to joint-limit, interference and possibly kinematic mobility constraints. Since Φ possesses a simple form for many systems including the SRR, a rapid optimization technique such as the conjugate-gradient search can be employed (Arora, 1989). The conjugate gradient algorithm minimizes a positive definite quadratic function. For a nonlinear function such as Eq. (28), the algorithm can be applied by interpreting the quadratic function as a second-order Taylor series approximation of the performance index Φ . This is a reasonable assumption for the kinematics-based performance index, which is composed of trigonometric functions.

Since this is a nonlinear optimization problem, local minima may exist in the search space. Practically, however, the existence of local minima is unlikely due to the small size of the search space. More complex and computationally expensive optimization methods which are robust to local minima were not considered, since computation speed is highly important for planetary exploration rovers. The algorithm is summarized in Fig 10.

5. Results

Simulation and experimental results of the articulated suspension control algorithm applied to the Jet

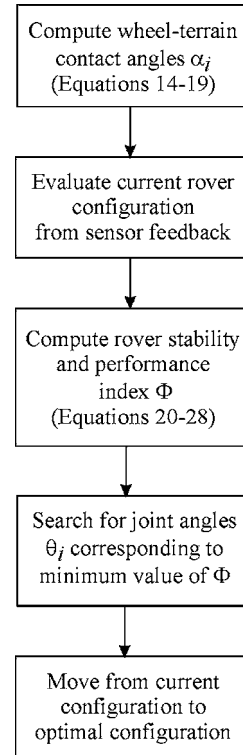


Figure 10. Algorithm summary diagram.

Propulsion Laboratory Sample Return Rover traversing rough terrain are presented below. The SRR is a 7 kg, four-wheeled mobile robot with independently driven wheels and independently controlled shoulder joints, see Fig. 1 (Huntsberger et al., 1999). A 2.25 kg three d.o.f. manipulator is mounted at the front of the SRR. The controllable shoulder joints and manipulator allow the SRR to reposition its center of mass. The SRR is equipped with an inertial navigation system to measure body roll and pitch. Since the ground speed of the SRR is typically 6 cm/sec, dynamic forces do not have a large effect on system behavior, and thus static analysis is appropriate.

The optimization performance index used in the simulation and experiments was similar to Eq. (28) and considered the two shoulder angle joints θ_1 and θ_2 and the three manipulator degrees of freedom ψ_1 , ψ_2 , and ψ_3 :

$$\Phi = \sum_{j=1}^4 \frac{K_j}{\eta_j} + \sum_{i=1}^2 K_{i+4}(\theta_i - \theta'_i)^2 \quad (29)$$

Note that the stability angles η_j are functions of the shoulder and the manipulator degrees of freedom (i.e., $\eta_j = \eta_j(\theta_1, \theta_2, \psi_1, \psi_2, \psi_3)$).

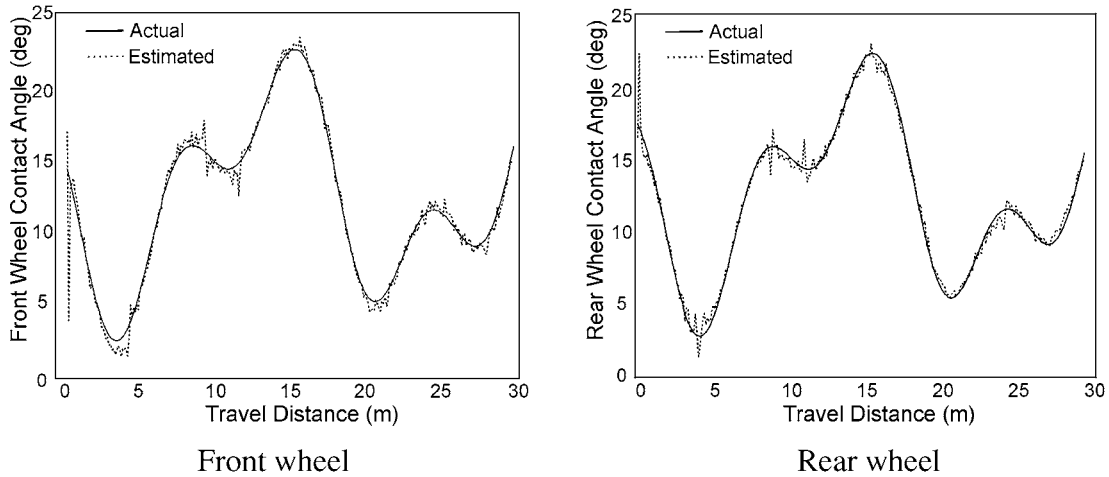


Figure 11. Simulated wheel-terrain contact angles and estimates for SRR front and rear wheels.

5.1. Simulation Results

The wheel-terrain contact angle estimation algorithm was implemented in simulation. The pitch α was corrupted with white noise of standard deviation 3° . The rear and front wheel velocities, v_1 and v_2 , were corrupted with white noise of standard deviation 0.5 cm/sec. This models error due to effects of wheel slip and tachometer noise.

Figures 11 and 12 show the results of a representative simulation trial. In Fig. 11 the actual and estimated wheel-terrain contact angles are compared. It can be seen that after an initial transient, the EKF estimate of the terrain contact angle is quite accurate, with RMS errors of 0.80° and 0.81° for the front and rear contact angles, respectively. Error increases at flat terrain regions (i.e., where the values of front and rear contact angles are identical) since the angle estimation equations become poorly conditioned due to reasons discussed previously. However, the error covariance matrix remained small during the simulation. In general, the EKF does an excellent job in simulation of estimating wheel-terrain contact angles in the presence of noise.

In Fig. 12, vehicle stability margin as defined by Eq. (25) is plotted for articulated suspension and fixed suspension systems. The mean stability of the articulated suspension system was 37.1% greater than the fixed suspension system. The stability margin of the fixed suspension system reaches a minimum value of 1.1° , indicating that the system narrowly avoided tipover failure. The minimum stability margin of the articulated suspension system was 12.5° , a comfortable margin.

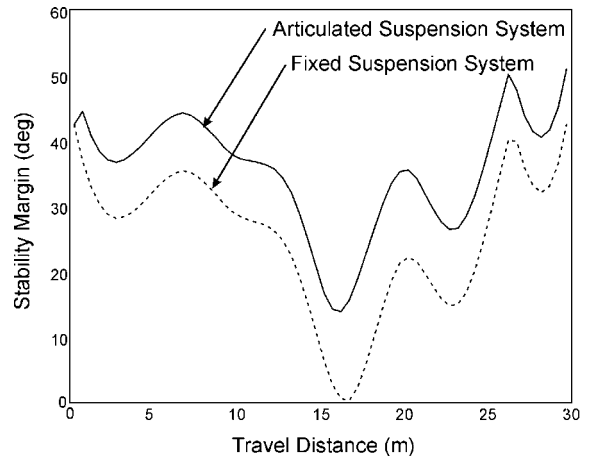


Figure 12. SRR stability margin for articulated suspension and fixed suspension system.

5.2. Experimental Results

Numerous experiments were performed on the SRR in the JPL Planetary Robotics Laboratory and at an outdoor rough-terrain test field, the Arroyo Seco in Altadena, California. The SRR was commanded to traverse a challenging rough-terrain path that threatened vehicle stability. For each trial the path was traversed first with the shoulder joints fixed, and then with the articulated suspension control algorithm activated. During these experiments, the SRR employed a state-machine control architecture, in which the vehicle traveled a small distance, stopped, then adjusted its shoulder angles based on the articulated suspension control algorithm. See Fig. 13 for images of the SRR during

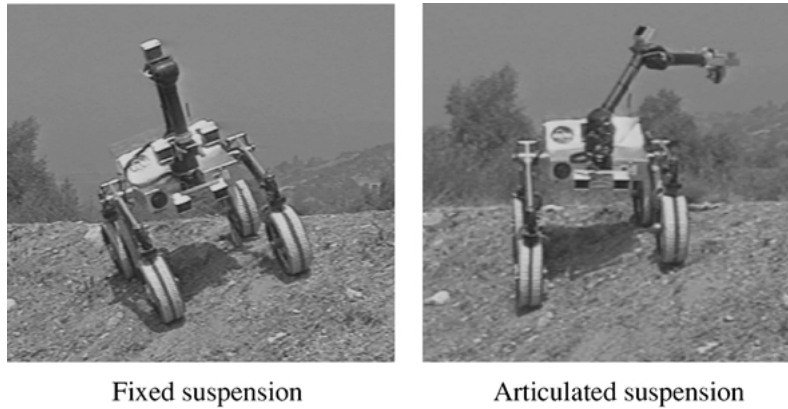


Figure 13. SRR during rough-terrain traverse.

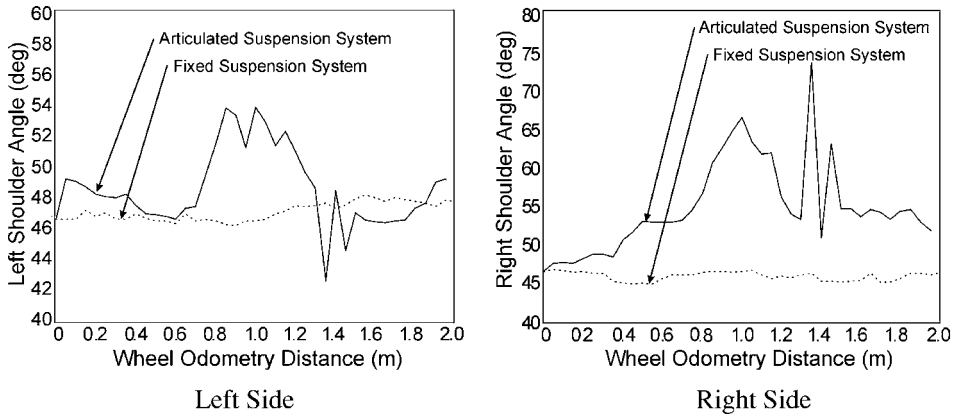


Figure 14. SRR shoulder angles during rough-terrain traverse for articulated suspension system and fixed suspension system.

a rough-terrain traverse with both fixed and articulated suspensions.

Results of a representative trial are shown in Figs. 14 and 15. Figure 14 shows the shoulder joint angles during the traverse. Both left and right shoulder angles remain within the joint limits of $\pm 45^\circ$ of the initial values. Note that the fixed suspension shoulder angles vary slightly due to servo compliance.

Figure 15 shows vehicle stability during the traverses. The average stability of the articulated suspension system was 48.1% greater than the fixed suspension system. The stability margin of the fixed suspension system reached dangerous minimum values of 2.1° and 2.5° . The minimum stability margin of the articulated suspension system was 15.0° . Clearly, articulated suspension control results in greatly improved stability in rough terrain.

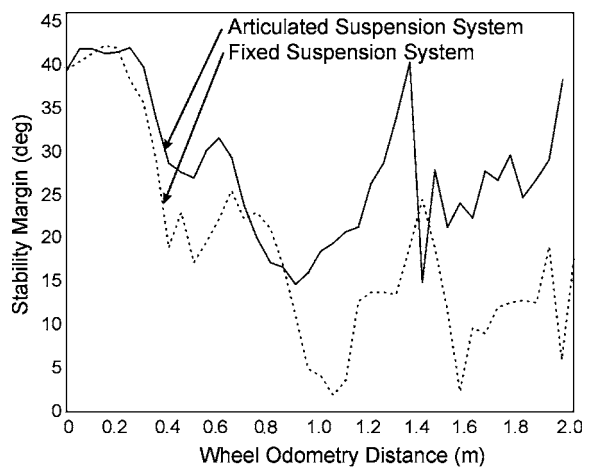


Figure 15. SRR stability margin for articulated suspension system and fixed suspension system on uneven terrain.

Optimization was performed on-line with a 300 MHz AMD K6 processor. Average processing time for a single constrained optimization computation was 40 μ sec. Thus, articulated suspension control greatly improves tipover stability in rough terrain and is feasible for on-board implementation.

6. Conclusions

A method for stability-based articulated suspension control has been presented. The method utilizes kinematic equations relating the suspension joint variables to the vehicle stability angles. A performance index based on these stability angles is optimized subject to vehicle constraints. This paper has also presented a wheel-ground contact angle estimation algorithm based on rigid-body kinematic equations. These angles are required to compute the locally optimal system configuration. The algorithm utilizes an extended Kalman filter to fuse on-board sensor signals. Simulation and experimental results for the JPL SRR show that the articulated suspension control method yields greatly improved vehicle stability in rough terrain.

Acknowledgments

The technical support of Paolo Pirjanian and Terrence Huntsberger of the JPL Planetary Robotics Laboratory is greatly appreciated. The authors would also like to thank Ken Waldron, Marco Meggiolaro, and Matt Lichter for their helpful contributions to this work. This research is supported by the NASA Jet Propulsion Laboratory under contract number 960456.

References

- Arora, J. 1989. *Introduction to Optimum Design*, McGraw-Hill: New York.
- Balaram, J. 2000. Kinematic state estimation for a mars rover. *Robotica*, 18:251–262.
- Brown, R. and Hwang, P. 1997. *Introduction to Random Signals and Applied Kalman Filtering*, John Wiley: New York.
- Eckhardt, H. 1989. *Kinematic Design of Machines and Mechanisms*, McGraw-Hill: New York.
- Farritor, S., Hacot, H., and Dubowsky, S. 1998. Physics-based planning for planetary exploration. In *Proceedings of the 1998 IEEE International Conference on Robotics and Automation*, pp. 278–283.
- Golombek, M. 1998. Mars pathfinder mission and science results. In *Proceedings of the 29th Lunar and Planetary Science Conference*.
- Hayati, S., Volpe, R., Backes, P., Balaram, J., and Welch, W. 1998. Microrover research for exploration of Mars. In *AIAA Forum on Advanced Developments in Space Robotics*.
- Huntsberger, T., Baumgartner, E., Aghazarian, H., Cheng, Y., Schenker, P., Leger, P., Iagnemma, K., and Dubowsky, S. 1999. Sensor fused autonomous guidance of a mobile robot and applications to Mars sample return operations. In *Proceedings of the SPIE Symposium on Sensor Fusion and Decentralized Control in Robotic Systems II*, Vol. 3839, pp. 2–8.
- Iagnemma, K. and Dubowsky, S. 2000. Vehicle wheel-ground contact angle estimation: With application to mobile robot traction control. In *Proceedings of the 7th International Symposium on Advances in Robot Kinematics, ARK '00*, pp. 137–146.
- Iagnemma, K., Rzepniewski, A., Dubowsky, S., Huntsberger, T., Pirjanian, P., and Schenker, P. 2000. Mobile robot kinematic reconfigurability for rough-terrain. In *Proceedings of the SPIE Symposium on Sensor Fusion and Decentralized Control in Robotic Systems III*, Vol. 4196.
- Julier, S. and Uhlmann, J. 1997. A new extension of the Kalman filter to nonlinear systems. In *Proceedings of AeroSense: The 11th International Symposium on Aerospace/Defence Sensing, Simulation and Controls*.
- Papadopoulos, E. and Rey, D. 1996. A new measure of tipover stability margin for mobile manipulators. In *Proceedings of the IEEE International Conference on Robotics and Automation*, pp. 3111–3116.
- Schenker, P., Sword, L., Ganino, G., Bickler, D., Hickey, G., Brown, D., Baumgartner, E., Matthies, L., Wilcox, B., Balch, T., Aghazarian, H., and Garrett, M. 1997. Lightweight rovers for Mars science exploration and sample return. In *Proceedings of SPIE XVI Intelligent Robots and Computer Vision Conference*, Vol. 3208, pp. 24–36.
- Schenker, P., Baumgartner, E., Lindemann, R., Aghazarian, H., Zhu, D., Ganino, A., Sword, L., Garrett, M., Kennedy, B., Hickey, G., Lai, A., Matthies, L., Hoffman, B., and Huntsberger, T. 1998. New planetary rovers for long range Mars science and sample return. In *Proceedings of the SPIE Conference on Intelligent Robotics and Computer Vision XVII*, Vol. 3522.
- Schenker, P., Pirjanian, P., Balaram, B., Ali, K., Trebi-Ollennu, A., Huntsberger, T., Aghazarian, H., Kennedy, B., Baumgartner, E., Iagnemma, K., Rzepniewski, A., Dubowsky, S., Leger, P., Apostolopoulos, D., and McKee, G. 2000. Reconfigurable robots for all-terrain exploration. In *Proceedings of the SPIE Conference on Sensor Fusion and Decentralized Control in Robotic Systems III*, Vol. 4196.
- Shoemaker, C. and Bornstein, J. 1998. Overview of the Demo III UGV program. In *Proceedings of the SPIE Conference on Robotic and Semi-Robotic Ground Vehicle Technology*, Vol. 3366, pp. 202–211.
- Sreenivasan, S. and Wilcox, B. 1994. Stability and traction control of an actively actuated micro-rover. *Journal of Robotic Systems*, 11(6):487–502.
- Sreenivasan, S. and Waldron, K. 1996. Displacement analysis of an actively articulated wheeled vehicle configuration with extensions to motion planning on uneven terrain. *ASME Journal of Mechanical Design*, 118(2):312–317.
- Welch, G. and Bishop, G. 1999. An introduction to the Kalman filter. Technical Report 95-041, Department of Computer Science, University of North Carolina at Chapel Hill.



Karl Iagnemma is a research scientist in the Mechanical Engineering department of the Massachusetts Institute of Technology. He received his B.S. degree *summa cum laude* in mechanical engineering from the University of Michigan in 1994, and his M.S. and Ph.D. from the Massachusetts Institute of Technology, where he was a National Science Foundation graduate fellow, in 1997 and 2001, respectively. He has been a visiting researcher at the Jet Propulsion Laboratory. His research interests include rough-terrain mobile robot control and motion planning, robot-terrain interaction, and robotic mobility analysis. He is a member of IEEE and Sigma Xi.



Adam K. Rzepniewski received his B.S. in mechanical engineering from the University of Notre Dame, South Bend, Indiana, in 1999, and his M.S. degree from the Massachusetts Institute of Technology, Cambridge, Massachusetts in 2001. He is currently a Research Assistant working towards his Doctorate degree at the Massachusetts Institute of Technology. His research interests include optimization, control, and simulation of robotic systems, with emphasis on autonomous control and discrete-event manufacturing systems.



Steven Dubowsky received his Bachelor's degree from Rensselaer Polytechnic Institute of Troy, New York in 1963, and his M.S.

and Sc.D. degrees from Columbia, University in 1964 and 1971. He is currently a Professor of Mechanical Engineering at M.I.T. He has been a Professor of Engineering and Applied Science at the University of California, Los Angeles, a Visiting Professor at Cambridge University, Cambridge, England, and Visiting Professor at the California Institute of Technology, University of Paris (VI), and Stanford. During the period from 1963 to 1971, he was employed by the Perkin-Elmer Corporation, the General Dynamics Corporation, and the American Electric Power Service Corporation. Dr. Dubowsky's research has included the development of modeling techniques for manipulator flexibility and the development of optimal and self-learning adaptive control procedures for rigid and flexible robotic manipulators. He has also made important contributions to the areas of field and space robotics. He has authored or coauthored nearly 100 papers in the area of the dynamics, control and design of high performance mechanical, electromechanical, and robotic systems. Professor Dubowsky is a registered Professional Engineer in the State of California and has served as an advisor to the National Science Foundation, the National Academy of Science/Engineering, the Department of Energy, the U.S. Army and industry. He has been elected a fellow of the ASME and IEEE. He is a member of Sigma Xi and Tau Beta Pi.



Paul S. Schenker is Manager, Mobility Systems Concept Development Section, Jet Propulsion Laboratory, California Institute of Technology, Pasadena, leading Institutional R&D in planetary mobility and robotics. His published research includes topics in robotic perception, robot control architectures, telerobotics/teleoperation, sensor fusion, and most recently, multirobot cooperation. He is the developer of various robotic systems that include the Field Integrated Design & Operations Rover (FIDO), Planetary Dexterous Manipulator (MarsArm, microArm), Robot Assisted Microsurgery System (RAMS), Robotic Work Crew (RWC), and All Terrain Explorer (ATE/Cliffbot), with resulting technology contributions to NASA missions. Dr. Schenker is active in the IEEE, Optical Society of America, and SPIE. He has served as an elected Board member and 1999 President of the last; he currently serves on the NAS/United States Advisory Committee to the International Commission for Optics.